THREE-DIMENSIONAL UNSTEADY STATOR-ROTOR INTERACTIONS IN A HIGH EXPANSION ORC TURBINE

Gustavo J. Otero R.[1*], Stephan H.H.J. Smit[1], Rene Pecnik[1]

[1] Process and Eneregy Department, Delft University of Technology, Delft, the Netherlands.
* Corresponding author: G.J.OteroRodriguez@tudelft.nl

ABSTRACT

This study presents the three-dimensional and unsteady simulation of a high-expansion cantilever ORC turbine which operates with toluene in the real gas region. To this end, the Reynolds-averaged Navier-Stokes (RANS) equations are solved. A multi-parameter equation of state (EoS) is applied to define the thermodynamic state. A flux-conservative assembling technique for the treatment of non-matching three-dimensional meshes is applied to account for the unsteady stator-rotor interaction. The simulations indicate strong three-dimensional and unsteady effects, especially in the rotor blade passage. Because of the highly supersonic flow at the stator divergent section, unsteady shock waves emanate from the stator trailing edge, which disturbs the flow field downstream in the rotor channel. The analysis on the third direction indicates that the blade profile at different span-wise location and blade height distribution need to be optimized to reduce losses — generated by flow separation, secondary flow, and shock-waves — and increase the power output of the simulated high-expansion cantilever ORC turbine.

1. INTRODUCTION

ORCs have been widely applied to convert energy from low-to-medium grade heat sources into electrical power. The thermal energy available from biomass combustion, solar radiation, geothermal reservoirs or waste heat from industrial processes, is arguably immense, but the low temperature of these heat sources — typically between 120 to 350 °C — is the main disadvantage for their conversion into electricity. The main distinction between a standard Rankine cycle and an ORC is the working fluid; an ORC utilizes an organic compound with a high molecular-weight. The working fluid represents an additional degree of freedom to the ORC system as it can be selected to best match the temperature at the heat source (Colonna et al. (2015)).

Another distinction of an ORC with respect to a Rankine cycle is the expansion process. The expansion takes place close to the working fluid's critical point, in the dense-vapor region, where the ideal gas assumption is invalid. Therefore, to accurately describe organic fluids, complex equations of states are necessary (Hoffren et al. (2002); Colonna et al. (2008); Guardone et al. (2013); Wheeler and Ong (2013)). Moreover, an organic fluid features a small specific enthalpy drop which results in few expansion stages with a large pressure ratio. As a consequence, the turbine has a highly supersonic flow at the stator exit. For these reasons, design diagrams and correlations of steam turbines are not suitable for ORC turbines.

Several degrees of complexity can be included during the design of ORC turbines. Numerous studies have gone into detail on this topic in terms of preliminary design methodologies (Casati et al. (2014) and Uusitalo et al. (2015)), shape optimization using CFD (Pasquale et al. (2013) and Pini et al. (2015)), and detail blade design applying the two-dimensional method of characteristics (MoC) (Anand et al. (2019)). These studies concentrated on delivering a turbine design at the meridional plane, neglecting the span-wise direction. This is an acceptable approximation for the stator nozzle. However, for the rotor — and more specifically for a radial-inflow turbine — the three-dimensional (3-D) effects can become significant depending on the conditions/fluid (Wheeler and Ong (2014)).

Many efforts in advancing the physical understanding of the fluid dynamic operation of ORC turbo-machinery expanding non-ideal fluids have been conducted using numerical calculations. Most CFD

simulations of ORC turbomachinery are under the assumption of steady-state with the implementation of the mixing plane boundary condition at the interface between the stator and the rotor, for example Harinck et al. (2013); Sauret and Gu (2014); Al Jubori et al. (2017). However, in this type of simulations, the unsteady information between the stator and rotor is lost. Several studies that compared both steady and unsteady simulations of an ORC turbine stage are Rubechini et al. (2013), Wheeler and Ong (2014) and White and Sayma (2016). Both studies reported a significant performance drop in the unsteady simulation compared to the steady computation using the mixing plane boundary condition between stator and rotor. Therefore, the unsteady stator/rotor interaction influences the ORC turbine performance.

Another flow feature of ORC turbines frequently overlooked is the 3-D effects, as only a handful of studies have accounted for them in their predictions. Instead, most calculations consider a two-dimensional (2-D) or a quasi 3-D (Q3D) domain, see Bülten et al. (2015) and Rinaldi et al. (2016). An article that does consider the full 3-D geometry of a high expansion ORC turbine is Harinck et al. (2013). Other authors — for example Rubechini et al. (2013), Wheeler and Ong (2014), and Al Jubori et al. (2017) — have also performed 3-D simulations of ORC turbine but mostly consist of standard radial inflow turbines with an expansion ratio less than 11.

This work shows for the first time, by means of 3-D calculations, an analysis of the unsteady phenomena — shock waves, viscous wakes, and shockwave-boundary layer interaction — in a high-expansion ratio ORC turbine. Therefore, we investigate the three-dimensional, supersonic (Mach $\approx$ 2.5), and highly unsteady flow of a radial-inflow single stage ORC turbine (expansion ratio $\approx$ 100) operating with toluene ($C_6H_5 - CH_3$) as the working fluid. An in-house unsteady RANS code — see Pecnik et al. (2012) — is used to solve the system coupled to the multi-parameter EoS from Lemmon and Span (2006), to capture the unsteady interactions of the turbomachine and to account for the dense-gas effects of toluene, respectively. A flux-conserved assembling technique for the treatment of non-matching mesh interfaces, see Rinaldi et al. (2015), is used to model the unsteady interaction between the stator and the rotor.

2. GEOMETRY AND NUMERICAL DOMAIN

We designed a cantilever — radial inflow-radial outflow — turbine geometry for the expansion conditions of a commercial ORC power unit by Tri-O-Gen BV in the Netherlands, with a nominal power output in the range of 130-170 kW. The turbine consists of 18 stator nozzles and 43 rotor blades. The diffuser is not taken into account in the present study. The working fluid is toluene with inlet condition close to the critical point; the reduced temperature and pressure are in the range of $T_{red} = [0.9, 1.0]$ and $p_{red} = [0.75, 0.85]$, respectively. Moreover, the rotational speed of the ORC turbine is in the range of 24 to 30 krpm.

To design the turbine stage, we used the MoC, as described by Anand et al. (2019), for the radial inflow supersonic stator and our in-house blade parametrization for the rotor; the latter is not reported in this article for the sake of conciseness. Cantilever turbines require an increase in flow area due to the expansion of the medium. However, an increase in flow area in the blade channel is hard to accommodate due to the high volume flow ratio of organic fluids and to the radial inflow configuration. The blade height distribution is the free parameter used to control the area ratio in the rotor passage.

This study aims to account for 3-D effects in a high expansion ratio ORC turbine and quantify the importance of the 3-D effects on the flow field and overall performance. Therefore, two types of simulations are performed: a quasi 3-D (Q3D) and a full 3-D (F3D) simulations. Due to the computational burden, the number of rotor blade was decreased to 36 to reduce the numerical domain, 2 rotor blade per stator nozzle (see figure 1a). A 2-D plane grid is generated at mid-span — constant for both simulation type to have a reasonable comparison — as depicted in figure 1a. The nozzle and blades boundary layers were generated using an O-type structured mesh and elements were clustered at the wall — controlled by hyperbolic tangent function — in order to achieve a $y^+ \approx 1$. A Q3D domain corresponds to the meridional plane utilizing a single cell in the span-wise direction. Therefore, it is not possible to observe 3-D effects

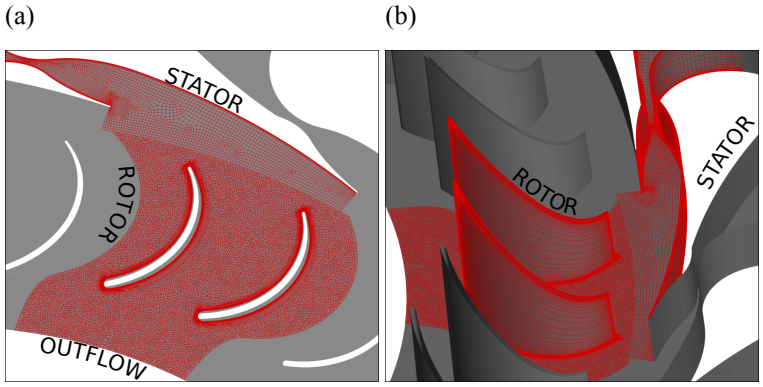

Figure 1 Numerical discretization of the computational domain: (a) 2D mesh, constant for all cases, and (b) F3D

in this type of domain. The cross-sectional area varies with the distance from the axis of rotation to allow the fluid to expand as in the 3-D geometry. A F3D simulation accounts for the whole blade passage in span-wise direction, using in our case 50 cells in this direction, see figure 1b, making it possible to estimate the flow behaviour in the direction normal to the meridional plane. The thickness of the blade varies from hub to shroud because of strength and vibrational purposes in the actual machine. Hence the rotor blade is thicker at the root and thinner at the shroud. Figure 1b also illustrates the sharp increase of height in the rotor channel. The discretization in the span-wise direction is made such that elements are cluster near the wall at the hub and the shroud, achieving a $y^+_{max} < 10$.

3. NUMERICAL METHODS

Solver: An in-house CFD code (see Pecnik et al. (2012)), which discretizes the compressible Navier-Stokes equation using the finite volume formulation, is used to simulate the high expansion ORC turbine. An approximate Riemann solver, AUSM$^+$ from Liou (1996), is used to approximate the advection term of the Navier-stokes equation. All simulations are performed using second-order spatial accuracy to reconstruct the face value of a given variable. A two-step Backward differentiation scheme is used to advance the simulation in time, solving the linear system with the Biconjugate Gradient Stabilized Method from Van der Vorst (1992).

Equation of state: The multi-parameter EoS of Lemmon and Span (2006) is used to represent the fluid properties. A look-up table for toluene is generated for a range of $T = [310, 390]$ K and $\rho = [0.005, 145.0]$ kg m^{-3} using 400 nodes for each axis. A uniform and a logarithmic spacing, for the temperature and the density, respectively, are used to discretize the thermodynamic table. The look-up table tabulates pressure, entropy, enthalpy, viscosity, thermal conductivity, and the speed of sound. We used a linear interpolation scheme, which for the tabulated region had a maximum interpolation error of 0.05 %.

Turbulence modelling: The one-equation turbulence model of Spalart and Allmaras (1992) is used to model the Reynolds stresses and close the system of equations. Other authors have used this eddy viscosity model for ORC turbomachinery, see Rinaldi et al. (2016); Wheeler and Ong (2014); Bülten et al. (2015). In our previous study, see Otero Rodriguez et al. (2018), this model gave accurate results when solving full developed channel flows with a strong variation on the thermo-physical properties if compared to direct numerical simulations.

Boundary conditions: In table 1, a summary of the boundary conditions is given. A fully conservative flux assembling technique for the treatment of non-matching mesh interfaces is used to model the unsteady stator-rotor interaction, see Rinaldi et al. (2015). The non-matching mesh technique was extended in this research to handle 3-D geometries.

Table 1: CFD boundary conditions. † For the F3D simulation, a zero angle in the spanwise direction of the velocity is set at the inflow. †† To initialize the flow field, a static pressure is prescribed at the outflow. For the turbulence model, an inflow value of the Spalart-Allamaras scalar is given. At the wall, the Spalart-Allamaras scalar is set to zero.

Type of domain	Inflow†	Outflow††	Walls	Top & bottom	ω [krpm]
Q3D	T_0, p_0, α	$\nabla p = 0$	No slip and adiabatic	$\nabla v_n = 0$	28
F3D				Adiabatic wall	

4. RESULTS

This section of the article reports the outcome from two unsteady ORC turbine simulations: a Q3D and an F3D simulation. We first examine the unsteadiness of the flow field with time-evolution contour plots. Afterward, we investigate the 3-D effects in the ORC turbine by comparing the two simulations.

4.1 Unsteady flow interaction

In figure 2, we present the time evolution of the relative Mach number with constant pressure lines. To avoid redundancy, we will only discuss the unsteady shock-wake interaction for the Q3D simulation. Moreover, we have limited our analysis to half the angular period — the rotation of one rotor blade — given the periodic nature of the flow field. In this plot, and in several contour plots in this paper, constant pressure lines in the range of 20 bar to 0.2 bar are illustrated as black continuous lines. A cluster of pressure lines represent a strong pressure gradient, which indicates a shock wave. Therefore, the unsteady interaction of shock waves and viscous wakes can be visualized using theses plots.

The flow features in the static domain are typical of a well-designed radial inflow supersonic stator vane. Because of the high expansion ratio of the turbine, the flow is accelerated to sonic conditions at the throat of the stator and later becomes supersonic in the divergent section. A highly supersonic flow is reached at the end of the nozzle, with a Mach number of around 2.7. There are two oblique shock-waves stemming from the stator trailing edge (STE), one enters directly towards the rotor and the other one hits the long stator wall which is then reflected towards the rotor, see a snapshot of the pressure gradient contour in figure 3a. Both shock-waves disturb the flow field downstream; however, these are weak oblique shocks and do not generate any recompression in the semi-bladed region between the stator and rotor. Thus the design of the stator blade achieves the desired expansion ratio.

The rotor blade suffers from several flow phenomena that increase losses. A bow shock-wave is produced at the rotor leading edge (RLE) because the flow is supersonic in the relative frame of reference; the flow at this location has a relative Mach number of 1.25. Moreover, the flow becomes detached in the suction side (SS) of the blade inducing a recirculation bubble and another oblique shock; the flow is still supersonic in the relative frame. Because of the increase of area in the blade channel, the flow continues to accelerate, reason why two oblique shocks emanate from the rotor trailing edge (RTE).

The unsteady nature of the flow is revealed between the stator and the rotor, and in the rotor blade passage, see figure 2. We can distinguish three unsteady structures in the flow field: (1) the viscous wake (VW) at the STE, (2) the bow shock (BS) at the RLE, and (3) the oblique shock (OS) emanating from the flow separation at the SS of the blade. Between stator and rotor, the flow field is unsteady as a result of the influence of the blade rotation on both the VW and the oblique shock-waves that emanate from the STE. The BS of the RTE of blade 2 interacts with the VW of the STE, see $\tau = 3/12$ to $\tau = 5/12$. This interaction continues until the wake enters the rotating domain, seen in $\tau = 1/12$ and $\tau = 2/12$ for the BS of the RTE of blade 1. From $\tau = 0/12$ we can see — between the pressure side (PS) of blade 1 and SS of blade 2 — how the BS and OS interact with each other. This shock-shock interaction is rotating with the flow, as seen in $\tau = 1/12 - 3/12$, until it impinges in blade 1 PS at $\tau = 4/12$. In $\tau = 5/12$ the three unsteady structures — BS, OS, and VW — are interacting near the RLE of blade 1. The detached

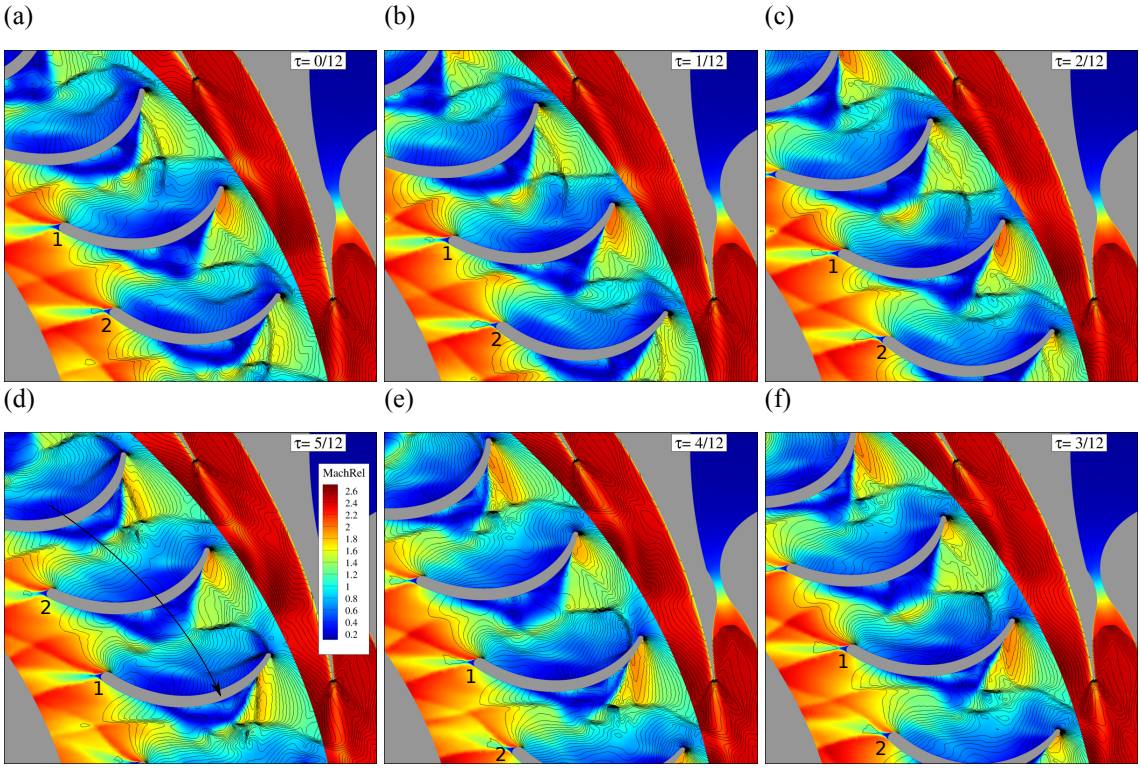

Figure 2 Time evolution of the relative Mach number with constant pressure lines for the Q3D numerical domain. The pressure lines goes from 20 bar at the stator divergent part to 0.2 bar at the exit of the blade channel.

flow in the SS of the blade is also unsteady, see for example in $\tau = 3/12$ and $\tau = 4/12$ how eddy induced shocks are emanating from the separation bubble of blade 1 SS. These eddy shocklets are created by the interaction of the VW with the rotor channel. The detailed study of high-expansion ORC turbines requires time-dependent simulations with a flux-conserving interface between stator and rotor.

4.2 Three-dimensional effects

The time-averaged entropy contours at mid-span of the Q3D and F3D simulations, see figures 4a and 4c, have similar flow field structures with disparities in the rotor. The flow field in the stator is not influenced by the three-dimensional effects. In the rotating domain, we can see that the shock-waves are weaker in the F3D simulation at mid-span, confirmed by the snapshot of the pressure gradient in figure 3. However, the bow shock in the F3D simulation is part of a larger 3-D shock as seen in figure 3c. The flow separation

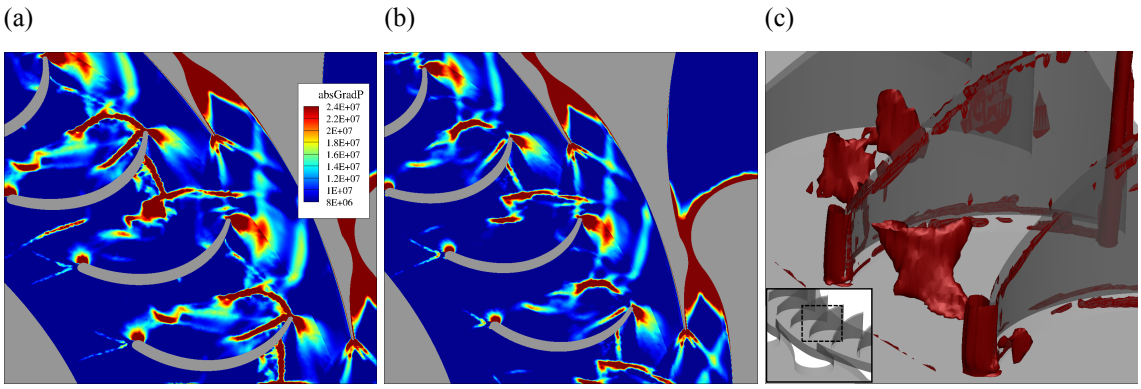

Figure 3 Snapshot of the magnitude of the pressure gradient field: (a) Q3D, (b) F3D with XY view, and (c) F3D with 3-D view: pressure gradient iso-surfaces = 3 10^7.

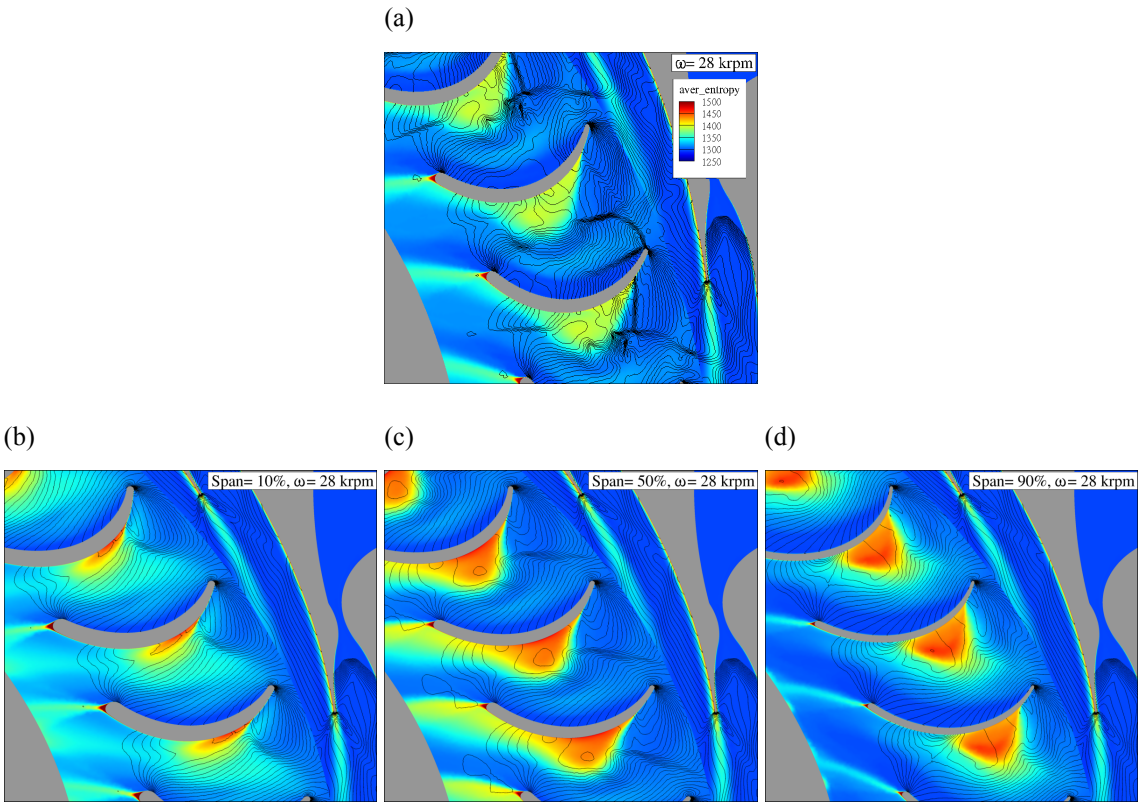

Figure 4 Time-averaged entropy contour with constant pressure lines for the (a) Q3D, and F3D numerical domain at three span-wise locations: (b) 10% span, (c) 50% span, and (d) 90% span. The pressure lines goes from 20 bar at the stator divergent part to 0.2 bar at the exit of the blade channel.

in the SS of the blade is present in both simulations. However, the F3D simulation has a higher entropy increase. These results already show that there exist substantial differences between a Q3D and F3D simulation of a high-expansion ratio ORC turbine.

The entropy at the mid-span section of the F3D simulation is always higher than for the Q3D simulation for the same shaft speed. Figure 5a gives a quantitative representation of the mass-averaged in time and space of the entropy as a function of the radius in the Q3D and F3D simulations; the latter only considers the mid-span section (35% to 70% span). There is not entropy difference in the stator until the throat. In the diverging part of the stator nozzle, there is an increase in the entropy for both simulation. Caused by the flow detachment, the blade channel is the section of the turbine where the highest increase in entropy is observed. The behavior of the averaged entropy distribution across the turbine stage is comparable between the two simulations — Q3D and F3D — at mid-span. In the stator nozzle, until the STE, both simulation types have equivalent entropy distribution. However, in the rotor channel, the F3D simulation has a higher entropy increase, especially near the RTE. From these results we can conclude that the 3-D effects have a substantial impact in terms of entropy across the rotor of a high-expansion ORC turbine.

A F3D simulation provides the possibility to investigate the flow of the turbine at all span-wise locations. In this regard, figure 4b)-d) describe the time-averaged entropy contours for the F3D simulations at three span-wise levels: 10% (near the hub), 50% (at mid-span), and 90% (near the shroud). A more quantitative description of the flow field is shown in figure 5b, where the mass-averaged in time and space of the entropy is plotted along the radius for the hub (mass averaging between 0% – 35% span), mid-span (35% – 65% span), and shroud (65% – 100% span) sections of the domain.

In terms of the flow field in the stator, figures 4b)-d), there is no change in the vertical direction. However,

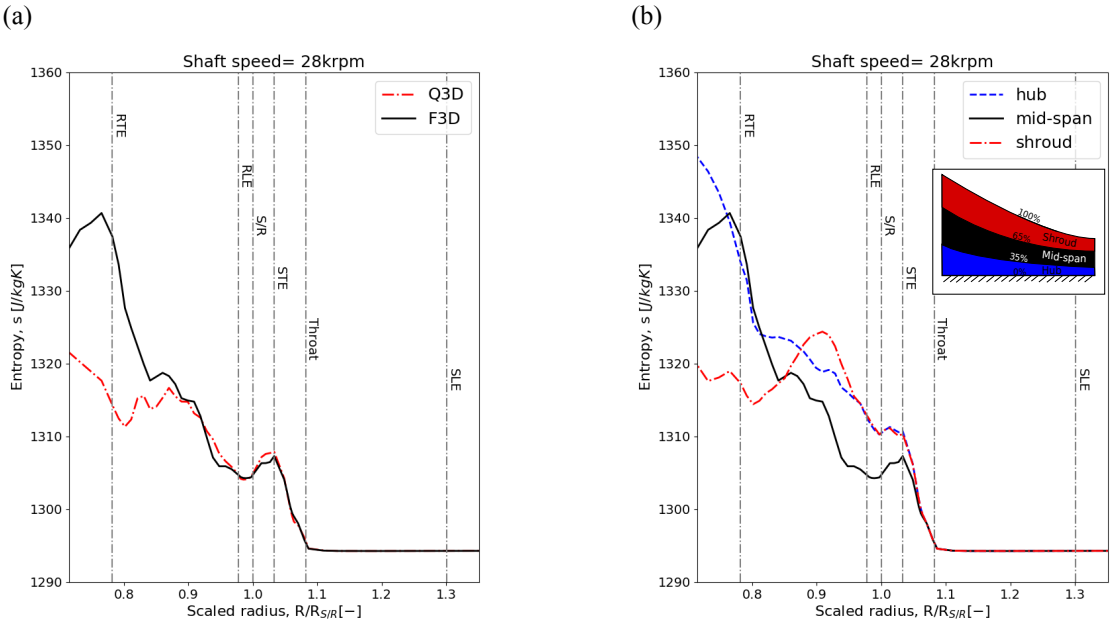

Figure 5 Time- and mass- averaged entropy along the radius of the turbine stage comparing: (a) Mid-span section of the F3D and Q3D simulations and (b) span-wise sections of the F3D simulation.

clear differences are seen in the averaged entropy for different span-wise locations, as shown by figure 5b. There is a larger increase in entropy after the STE, near the hub and the shroud, as a consequence of the boundary layer formation at the top and bottom stator walls. Still, the nozzle vane can be designed at mid-span without any consequence in the third direction.

Large differences in the flow field are observed in the span-wise direction at the rotor channel, see figures 4b)-d). Three important flow features change along the span-wise direction: (1) the size and location of the recirculation in the SS of the blade, (2) the strength of the bow shock at the RLE, and (3) the viscous wake of the RTE. Therefore, to have a well-designed rotor of the simulated high-expansion ORC turbine, the blade profile needs to be adapted in the third direction to account for these changes of the flow field.

Contrary to the mid-span, the entropy increase at the hub are not restricted to the recirculation bubble, compare for example the rotor channel in figures 4b and 4c. Quantitatively, the hub is the section of the domain with the highest increase in entropy as seen in figure 5b. These discrepancies between the mid-span and hub are a consequence of the boundary layer at the hub wall.

The flow field near the blade shroud has the highest difference if compared to the mid-span. The flow detachment has change in location relative to the chord distance of the blade; the separation bubble at the shroud is closer to the RLE, see figure 4d. Moreover, the shape of the flow separation at the shroud is distinct. Figure 6 depicts the reason for these differences: secondary flow caused by the high flaring angle of the blade height distribution. The high flaring angle of the height distribution is a consequence of (1) the radial inflow configuration, and (2) the high volume flow ratio. Therefore, the height distribution needs to increase rapidly in the rotor channel to compensate for these two factors. The high flaring angle in the radial-to-axial bend drives low momentum fluid towards the shroud because of the meridional stream-wise curvature in the span-wise direction. Regarding figure 5b, the entropy increase in the shroud is equivalent to the hub — due to the already discuss near-wall effects — until the height distribution starts to change in the rotor channel. A sharp increase in the averaged entropy — due to the secondary flow — is seen just at the inlet of the rotor channel for the shroud section. The blade design of the simulated high-expansion ORC turbine needs to consider the span-wise direction effects, a consequence

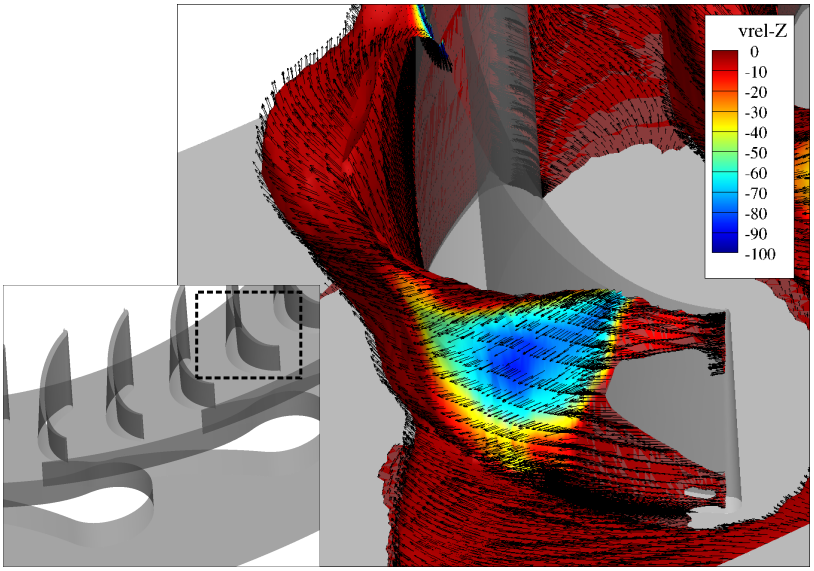

Figure 6 Entropy iso-surface snapshot with a contour of the relative velocity in the z-direction. Vectors represent the relative velocity field.

of a high flaring angle of the height distribution, as they decrease the performance of the turbine.

The F3D calculations give a worse performance of the high-expansion ORC turbine compared to the Q3D counterpart for all simulated shaft speeds. We have measured the performance of the ORC turbine by means of the power output, and the isentropic and total-to-static efficiency. There is a 3.15% and 1.19% drop on the F3D simulation relative to isentropic and total-to-static efficiency of the Q3D simulation ($\Delta\eta = \eta_{Q3D} - \eta_{F3D}$), respectively, resulting in less power output: -15.3kW. The additional loss mechanisms, quantifiable by a F3D simulation, decrease the performance of the high-expansion ORC turbine stage.

5. CONCLUSIONS

Utilizing detailed RANS simulations, we investigated the three-dimensional, supersonic, and highly unsteady flow of a high-expansion ratio ORC turbine operating with toluene as the working fluid. We performed two types of numerical simulations, a quasi-three-dimensional and a full three-dimensional calculations. Because the fluid expansion takes place close to the dense-vapor region, the fluid's thermodynamic properties were evaluated with a multi-parameter equation of state. In this original research, we investigated for the first time the unsteady phenomena of a high-expansion ORC turbine via three-dimensional calculations.

In our analysis, we illustrated the most relevant aerodynamic features that need to be addressed when designing a high-expansion ORC turbine. Between the stator and the rotor, there is a strong coupling between the shock-waves and viscous wake emanating from the stator trailing edge, and the rotation of the blades. These unsteady phenomena, emerging from the stator, modified the flow field downstream in the rotor channel. Moreover, we observed flow detachment at the suction side of the blade that generate a large entropy increase. The designer of the high-expansion ORC turbine needs to analyze the effect of the height distribution relative to secondary flow at the rotor channel. The three-dimensional effects resulted in a drop in performance, as a consequence of the loss mechanisms quantifiable only with a three-dimensional simulation: the hub and shroud boundary layer, and a secondary flow in the blade channel.

NOMENCLATURE

Acronyms			
2-D	two-dimensional	SLE	stator leading edge
3-D	three-dimensional	SS	suction side
BS	bow shock-wave	STE	stator trailing edge
CFD	computational fluid dynamics	VW	viscous wake
EoS	Equation of State	**Symbols**	
F3D	full three-dimensional	p	pressure
MoC	Method of Characteristics	T	temperature
ORC	organic Rankine cycle	v	velocity
OS	oblique shock-wave	**Greek letters**	
PS	pressure side	α	velocity angle
Q3D	quasi-three-dimensional	ρ	density
RANS	Reynolds-averaged Navier-Stokes	τ	time period
RLE	rotor leading edge	**Subscript**	
RTE	rotor trailing edge	0	total conditions
		n	normal direction

REFERENCES

Al Jubori, A., Al-Dadah, R. K., Mahmoud, S., Ennil, A. B., and Rahbar, K. (2017). Three dimensional optimization of small-scale axial turbine for low temperature heat source driven organic Rankine cycle. *Energy conversion and management*, 133:411–426.

Anand, N., Vitale, S., Pini, M., Otero, G. J., and Pecnik, R. (2019). Design methodology for supersonic radial vanes operating in nonideal flow conditions. *Journal of Engineering for Gas Turbines and Power*, 141(2):022601.

Bülten, B., Althaus, W., Weidner, E., and Stoff, H. (2015). Experimental and numerical flow investigation of a centripetal supersonic turbine for organic Rankine cycle applications. In *11th European Conference on Turbomachinery Fluid Dynamics and Thermodynamics, Madrid, Spain, March 2015*, pages 23–27. ASME.

Casati, E., Vitale, S., Pini, M., Persico, G., and Colonna, P. (2014). Centrifugal turbines for mini-organic Rankine cycle power systems. *Journal of Engineering for Gas Turbines and Power*, 136(12):122607.

Colonna, P., Casati, E., Trapp, C., Mathijssen, T., Larjola, J., Turunen-Saaresti, T., and Uusitalo, A. (2015). Organic Rankine cycle power systems: from the concept to current technology, applications, and an outlook to the future. *Journal of Engineering for Gas Turbines and Power*, 137(10):100801.

Colonna, P., Harinck, J., Rebay, S., and Guardone, A. (2008). Real-gas effects in organic Rankine cycle turbine nozzles. *Journal of Propulsion and Power*, 24(2):282–294.

Guardone, A., Spinelli, A., and Dossena, V. (2013). Influence of molecular complexity on nozzle design for an organic vapor wind tunnel. *Journal of engineering for gas turbines and power*, 135(4):042307.

Harinck, J., Pasquale, D., Pecnik, R., van Buijtenen, J., and Colonna, P. (2013). Performance improvement of a radial organic Rankine cycle turbine by means of automated computational fluid dynamic design. *Proceedings of the Institution of Mechanical Engineers, Part A: Journal of Power and Energy*, 227(6):637–645.

Hoffren, J., Talonpoika, T., Larjola, J., and Siikonen, T. (2002). Numerical simulation of real-gas flow in a supersonic turbine nozzle ring. *Journal of engineering for gas turbines and power*, 124(2):395–403.

Lemmon, E. W. and Span, R. (2006). Short fundamental equations of state for 20 industrial fluids. *Journal of Chemical & Engineering Data*, 51(3):785–850.

Liou, M.-S. (1996). A sequel to AUSM: AUSM$^+$. *Journal of computational Physics*, 129(2):364–382.

Otero Rodriguez, G., Patel, A., Diez Sanhueza, R., and Pecnik, R. (2018). Turbulence modelling for flows with strong variations in thermo-physical properties. *International Journal of Heat and Fluid Flow*, 73.

Pasquale, D., Ghidoni, A., and Rebay, S. (2013). Shape optimization of an organic Rankine cycle radial turbine nozzle. *Journal of Engineering for Gas Turbines and Power*, 135(4):042308.

Pecnik, R., Terrapon, V. E., Ham, F., Iaccarino, G., and Pitsch, H. (2012). Reynolds-averaged navier-stokes simulations of the Hyshot II scramjet. *AIAA journal*, 50(8):1717–1732.

Pini, M., Persico, G., Pasquale, D., and Rebay, S. (2015). Adjoint method for shape optimization in real-gas flow applications. *Journal of Engineering for Gas Turbines and Power*, 137(3):032604.

Rinaldi, E., Colonna, P., and Pecnik, R. (2015). Flux-conserving treatment of non-conformal interfaces for finite-volume discretization of conservation laws. *Computers & Fluids*, 120:126–139.

Rinaldi, E., Pecnik, R., and Colonna, P. (2016). Unsteady operation of a highly supersonic organic rankine cycle turbine. *Journal of turbomachinery*, 138(12):121010.

Rubechini, F., Marconcini, M., Arnone, A., Del Greco, A. S., and Biagi, R. (2013). Special challenges in the computational fluid dynamics modeling of transonic turbo-expanders. *Journal of Engineering for Gas Turbines and Power*, 135(10):102701.

Sauret, E. and Gu, Y. (2014). Three-dimensional off-design numerical analysis of an organic Rankine cycle radial-inflow turbine. *Applied Energy*, 135:202–211.

Spalart, P. and Allmaras, S. (1992). A one-equation turbulence model for aerodynamic flows. In *30th aerospace sciences meeting and exhibit*, page 439.

Uusitalo, A., Turunen-Saaresti, T., Gronman, A., Honkatukia, J., and Backman, J. (2015). Combined thermodynamic and turbine design analysis of small capacity waste heat recovery ORC. *Proceedings of the ASME ORC*.

Van der Vorst, H. A. (1992). Bi-CGSTAB: A fast and smoothly converging variant of Bi-CG for the solution of nonsymmetric linear systems. *SIAM Journal on scientific and Statistical Computing*, 13(2):631–644.

Wheeler, A. P. and Ong, J. (2013). The role of dense gas dynamics on organic Rankine cycle turbine performance. *Journal of Engineering for Gas Turbines and Power*, 135(10):102603.

Wheeler, A. P. and Ong, J. (2014). A study of the three-dimensional unsteady real-gas flows within a transonic ORC turbine. In *ASME Turbo Expo 2014: Turbine Technical Conference and Exposition*, pages V03BT26A003–V03BT26A003. American Society of Mechanical Engineers.

White, M. and Sayma, A. (2016). Investigating the effect of changing the working fluid on the three-dimensional flow within organic Rankine cycle turbines. In *ASME Turbo Expo 2016: Turbomachinery Technical Conference and Exposition*, pages V003T25A002–V003T25A002. American Society of Mechanical Engineers.

ACKNOWLEDGEMENT

The authors thank the Netherlands Organization for Scientific Research (NWO) who funded this research through the grant with project number 14711.